Noise Modelling and Uncertainty Propagation for TOF Sensors

Amira Belhedi[1,2,3], Adrien Bartoli[2], Steve Bourgeois[1], Kamel Hamrouni[3], Patrick Sayd[1], and Vincent Gay-Bellile[1]

[1] CEA, LIST, LVIC
[2] Clermont Université, Université d'Auvergne, ISIT
[3] Université de Tunis El Manar, ENIT, SITI
{amira.belhedi,Vincent.Gay-Bellile,Steve.Bourgeois,Patrick.Sayd}@cea.fr,
adrien.bartoli@gmail.com, kamel.hamrouni@enit.rnu.tn

Abstract. Time-of-Flight (TOF) cameras are active real time depth sensors. One issue of TOF sensors is measurement noise. In this paper, we present a method for providing the uncertainty associated to 3D TOF measurements based on noise modelling. Measurement uncertainty is the combination of pixel detection error and sensor noise. First, a detailed noise characterization is presented. Then, a continuous model which gives the noise's standard deviation for each depth-pixel is proposed. Finally, a closed-form approximation of 3D uncertainty from 2D pixel detection error is presented. An applicative example is provided that shows the use of our 3D uncertainty modelling on real data.

1 Introduction

Time-of-Flight (TOF) cameras open new possibilities in fields such as 3D reconstruction, Augmented Reality and video-surveillance since they provide depth information in real-time and at high frame-rates. They are based on the emission of a modulated infrared light which is thereafter reflected by the objects in the scene. The signal's phase shift φ is determined and thus the depth value d by a TOF approach [1]. The depth value, at each pixel, is given by $d = \frac{c\varphi}{4\pi\omega}$, where c is the speed of light and ω is the modulation frequency. This technology has several limitations, one of them being measurement noise. During the past years, some works [2–5] have been devoted to enhancing the depth images captured by a TOF sensor by handling the noise. However, there have been no studies of noise that provides the TOF measurements uncertainty.

In this paper, we characterize the noise distribution as Gaussian (Section 2). We show that its standard deviation varies according to the pixel position and the depth. We propose a continuous noise modelling which gives the noise's standard deviation for each depth-pixel (Section 3). Our model uses a 3D smoothing spline, known as a 3D Thin-Plate Spline, known to work well to model complex variations. Generally speaking, a measurement is meaningful only if its uncertainty can be compute as well. We present a method for providing 3D uncertainty for TOF sensors (Section 4). The 3D uncertainty in TOF measurements is the

A. Fusiello et al. (Eds.): ECCV 2012 Ws/Demos, Part III, LNCS 7585, pp. 476–485, 2012.

combination of pixel detection error and sensor noise. We describe how errors in 2D measurements propagate to error in the 3D measurements, and hence we are able to compute a confidence interval on any 3D measurement, *i.e.* a quantitative assessment of accuracy. The proposed method is a closed-form approximation from 2D pixel detection error and a continuous depth noise model. The work has a variety of applications. We present an applicative example in Section 5.

Notation. A 2D point $\mathbf{p}$ (pixel) is the 2-vector defined as $\mathbf{p}^\mathsf{T} = (u \quad v)$ with $(u \ v)$ the pixel coordinates, a 2.5D point $\mathbf{q}$ (depth-pixel) is the 3-vector defined as $\mathbf{q}^\mathsf{T} = (u \quad v \quad d)$ with d the associated depth and the corresponding 3D point in the camera coordinate frame is $\mathbf{Q}^\mathsf{T} = (X \quad Y \quad Z)$.

2 Noise Characterization

The noise characterization is based on the study of the variation on the depth-pixel measurements for several TOF images taken in the same conditions. Images of a white wall were acquired at 7 depths from 0.9 m to 7.4 m. At each depth, 100 depth images were recorded. To characterize the noise distribution, we used the technique of normal probability plot [6]. The data are plotted against a theoretical normal distribution in such a way that the points should form an approximate straight line. Departures from this straight line indicate departures from normality. An example corresponding to a depth-pixel (Figure 5) shows that the scatter follows approximately straight lines. To verify graphically the normality of the noise distribution for more pixels, the images' centers are considered. Their associated histograms showing the distribution of the depth measurements are plotted in Figure 1. These histograms, as can be graphically seen, follow a Gaussian distribution. After the graphical verification, a more robust Gaussian test was used. The Lilliefors (adaptation of the Kolmogorov-Smirnov [1]) tests the null hypothesis that the data comes from a distribution in the normal family. The test returns the logical value $h = 1$ if it rejects the null hypothesis, otherwise it returns $h = 0$. This test is performed for each pixel of the 7 depths, then the median and mean value of h for all pixels are computed. The median value is equal to 0 and the mean value is also 'near' zero (equal to 0.1472). These values confirm that the TOF noise follows a Gaussian distribution to a good extent. We are now interested in noise variation according to pixel position and depth. The standard deviation σ is calculated for each pixel of the 7 images. Figure 2 present σ values at each pixel for an approximative depth $d = 4.23m$. As can be clearly seen, σ increases away from the image center (5 to 7 mm) to the image boundaries (7 to 27 mm). The highest accuracy is achieved at the image center where the illumination of the observed object is at its highest value. The same phenomenon is observed for the other 6 depths. The standard deviation dependency on the depth is shown in Figure 3. The σ at each pixel of the 7 depths is calculated and plotted against the depths values. σ increases with depth and

[1] The Kolmogorov-Smirnov test is used to decide if a sample comes from a population with a specific distribution.

varies approximately from 0 to 40 mm (the mean value of σ is 8 mm) as shown in Figure 4. The noise's standard deviation gives an information about the accuracy of measurement. This information is essential in any application, since it denotes the degree to which a measurement result will represent the true value. The calculated standard deviation from the 7 depths is however not sufficient. In practice, it is important to have a continuous noise modelling.

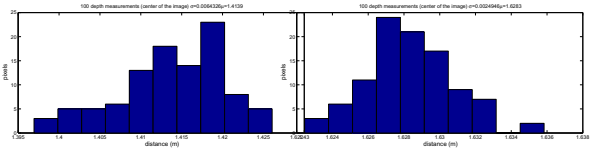

(a) Depth approx. 1.41m (b) Depth approx. 1.63m

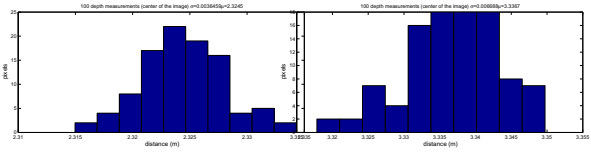

(c) Depth approx. 2.32m (d) Depth approx. 3.34m

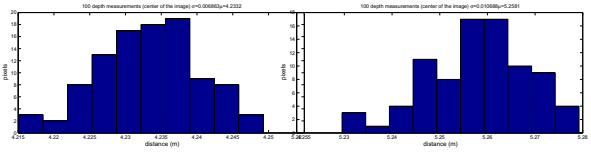

(e) Depth approx. 4.23m (f) Depth approx. 5.26m

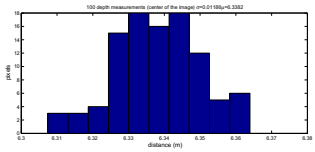

(g) Depth approx. 6.34m

Fig. 1. Noise's standard deviation distribution graphs. Each graph represents the distribution of the 100 depth measurements of the image center (of a white wall). Graphically, these histograms correspond to Gaussian distribution, as confirmed by the Kolmogorov-Smirnov test.

3 A Continuous Noise Modelling

The TOF noise has a Gaussian distribution, thus, the proposed noise modelling is based on standard deviation. The noise's standard deviation depends on both the pixel position and the depth. These variations cannot be well modelled by a simple constant or linear function. A more complex model is needed. It must also provide continuity, since it must give for each depth-pixel (2.5D point)

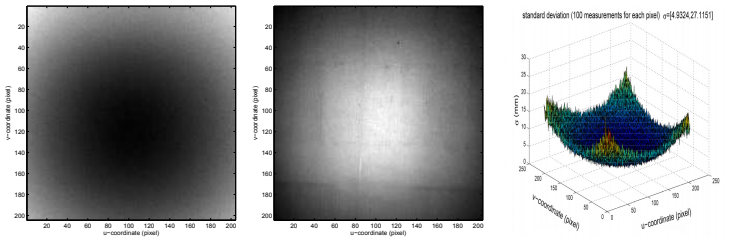

(a) depth image (b) intensity image (c) standard deviation

Fig. 2. Standard deviation σ (c) of a depth image (a) (of a white wall (b) at approx. 4.23 m) measured at each pixel. It is calculated out of 100 depth measurements at each pixel. σ increases from the image center (5 to 7 mm) to the image boundaries (7 to 27 mm).

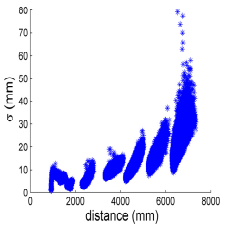

Fig. 3. The standard deviation calculated at each pixel of the 7 depths (of a white wall). σ is calculated out of 100 depth measurements at each pixel.

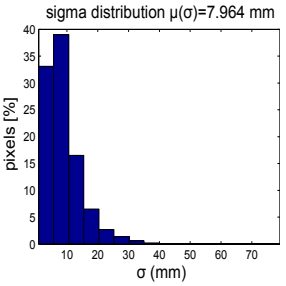

Fig. 4. Distribution of standard deviation calculated at each pixel of the 7 depths (of a white wall). σ is calculated out of 100 depth measurements at each pixel. σ increases with depth from 0 to 40 mm with a mean value equal to 8 mm.

the associated noise's standard deviation. A 3D Thin-Plate-Spline function is therefore chosen, since it verifies all these conditions. The 3D-TPS $\mathbb{R}^3 \rightarrow \mathbb{R}$ is a smooth function [7] known to be an efficient approximation to several types of deformation that minimizes the 'bending energy'. It is flexible, controlled by l 3D centers $\mathbf{c}_k$ ($\mathbf{c}_k \in \mathbb{R}^3, k = 1, \ldots, l$) that may be placed anywhere in space

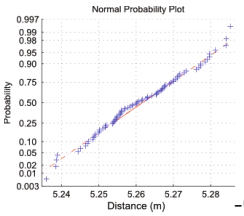

-0.2 in

Fig. 5. Normal probability plot corresponding to a depth-pixel. The scatter (plotted in blue) follows approximatively the straight line of the theoretical normal distribution (plotted in red).

and is driven by assigning target values α_k to the l 3D centers $\mathbf{c}_k$. It is usually parametrized by an $l+4$ coefficient vector $\mathbf{h}^\mathsf{T} = (\ \mathbf{w}^\mathsf{T}\ \ \mathbf{a}^\mathsf{T}\ )$ computed from the target vector α (described in the following) and a regularization parameter $\lambda \in \mathbb{R}^+$. There are l coefficients in $\mathbf{w}$ and 4 coefficients in $\mathbf{a}$. The coefficients in $\mathbf{w}$ must satisfy $\check{\mathsf{P}}^\mathsf{T}\mathbf{w} = \mathbf{0}$, where the k^{th} row of $\check{\mathsf{P}}^\mathsf{T}$ is given by $\left(\mathbf{c}_k^\mathsf{T}\ 1\right)$. These 4 'side-conditions' ensure that the TPS has square integrable second derivatives. Let $\boldsymbol{\ell}_\mathbf{q}^\mathsf{T} = ((d(\mathbf{q},\mathbf{c}_1))\ \cdots\ (d(\mathbf{q},\mathbf{c}_l))\ \ \mathbf{q}^\mathsf{T}\ 1)$, the 3D-TPS at a point $\mathbf{q}$ is given by:

$$\omega(\mathbf{q},\mathbf{h}) = \boldsymbol{\ell}_\mathbf{q}^\mathsf{T}\mathbf{h} = \left(\sum_{k=1}^{l} \mathbf{w}_k d(\mathbf{q},\mathbf{c}_k)\right) + \mathbf{a}^\mathsf{T}\check{\mathbf{q}}. \tag{1}$$

where $d(\mathbf{q},\mathbf{c}_k)$ is the distance between $\mathbf{q}$ and $\mathbf{c}_k$.

We use the 3D-TPS to model the Gaussian noise's standard deviation by defining a set of l centers positioned throughout the working volume (Figure 6). This parametric function is chosen for many reasons. First, it efficiently approximates the noise's standard deviation being considered as a deformation. Second, it limits the memory requirement, in fact, only the $l+4$ parameters and the l centers have to be saved. The proposed model is based on the standard deviation and defined by the function f:

$$\begin{aligned} f:\ \ \Omega \quad &\to \mathbb{R} \\ \begin{pmatrix} u \\ v \\ d \end{pmatrix} &\to \sigma\,, \end{aligned} \tag{2}$$

where $\Omega \subset \mathbb{R}^3$, $\Omega = [u_{min}; u_{max}] \times [v_{min}; v_{max}] \times [d_{min}; d_{max}]$ and σ is a scalar that represents the standard deviation. $f(\mathbf{q}) \stackrel{\text{def}}{=} \boldsymbol{\ell}_\mathbf{q}^\mathsf{T}\mathbf{h}$ and f lies in $L^2(\psi)$ [2]. The $l+4$ TPS coefficients in $\mathbf{h}$ are computed from the target σ_k (the standard deviation). Applying the TPS Equation (1) to the center c_r with target values σ_r gives:

$$\left(\sum_{k=1}^{l} \mathbf{w}_k d(\mathbf{c}_r,\mathbf{c}_k)\right) + \mathbf{a}^\mathsf{T}\check{\mathbf{c}}_r = \sigma_r. \tag{3}$$

[2] The Hilbert space of square-integrable functions.

Combining the equations obtained for all the l centers with the side-conditions in a single matrix equation gives:

$$\underbrace{\begin{pmatrix} \mathsf{K}_\lambda & \mathbf{P} \\ \mathbf{P}^\mathsf{T} & 0 \end{pmatrix}}_{\mathsf{D}} \underbrace{\begin{pmatrix} \mathbf{w} \\ \mathbf{a} \end{pmatrix}}_{\mathbf{h}} = \begin{pmatrix} \sigma \\ \mathbf{0} \end{pmatrix} \text{ with } \mathsf{K}_\lambda = \begin{cases} \lambda & r = k \\ d(\mathbf{c}_r, \mathbf{c}_k) & r \neq k. \end{cases} \tag{4}$$

In practice, we set λ to some small value such as $\lambda = 10^{-4}$, to ensure that K_λ and thus D are well conditioned. This is a linear system, the TPS coefficients in $\mathbf{h}$ are thus easily solved.

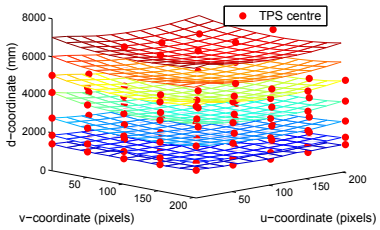

Fig. 6. The 7 depth images plotted together with the 3D TPS centers

4 Propagating Pixel Uncertainty to 3D

Pixel detection and extraction, whether manual or automatic, can only be performed to a finite accuracy. In addition to pixel detection error, depth-pixel extracted from TOF images are subject to sensor noise. One objective here is to consider how these errors propagate through the measurement formulas in order to quantify the uncertainty on the final 3D measurements. This is based on noise modelling. We concentrate in geometric measurements like object width and height, although, the method is not limited to those. This is achieved by using a first order error analysis. From pixels detected or clicked in the image, we want to estimate the geometric measurement and its uncertainty by propagating the uncertainty from the 2D point $\mathbf{p}$ to a 3D point $\mathbf{Q}$. We proceed in three steps: the first one is the uncertainty propagation from 2D (a pixel $\mathbf{p}$) to 2.5D ($\mathbf{q}$), the second one is the uncertainty propagation from 2.5D (corresponding point $\mathbf{q}$) to 3D (corresponding point $\mathbf{Q}$) and the third one is the uncertainty propagation from 3D to the final geometric measurement.

4.1 Propagating Pixel Uncertainty to 2.5D

The uncertainty of a 2D point $\mathbf{p}$ is the click or the detection error. This error is defined by the variance matrix on $\mathbf{p}$ denoted by $\Sigma^\mathbf{p}$ (2×2 matrix). We suppose that $\Sigma^\mathbf{p}$ is given. We define the transformation $T1$ between $\mathbf{p}$ and $\mathbf{q}$:

$$T1: \quad \Gamma \quad \rightarrow \Omega$$
$$\begin{pmatrix} u \\ v \end{pmatrix} \rightarrow \begin{pmatrix} u \\ v \\ d \end{pmatrix}, \tag{5}$$

where $d = d(u, v)$ and $\Gamma = [u_{min}; u_{max}] \times [v_{min}; v_{max}]$ defined by the image resolution.

A first order approximation for the variance-covariance matrix $\Sigma^{\mathbf{q}}_{inter}$ of $\mathbf{q}$ is given by:

$$\Sigma^{\mathbf{q}}_{inter} = \mathsf{J}_{T1} \Sigma^{\mathbf{p}} {\mathsf{J}_{T1}}^{\mathsf{T}}, \tag{6}$$

where J is the 3×2 Jacobian matrix of the function $T1$ defined as:

$$J_{T1} = \begin{pmatrix} 1 & 0 \\ 0 & 1 \\ d(u+1,v) - d(u,v) & d(u,v+1) - d(u,v) \end{pmatrix}, \tag{7}$$

4.2 Propagating 2.5D Uncertainty to 3D

In addition to the uncertainty of a 2D point detection, there is the uncertainty of the depth measurement. It is defined by the standard deviation σ modelled by the 3D TPS function f (Equation (2)). Incorporating the depth variance σ^2 in the variance-covariance matrix $\Sigma^{\mathbf{q}}_{inter}$ gives:

$$\Sigma^{\mathbf{q}} = \Sigma^{\mathbf{q}}_{inter} + \begin{pmatrix} 0\,0 & 0 \\ 0\,0 & 0 \\ 0\,0 & \sigma^2 \end{pmatrix}, \tag{8}$$

We show in the following that a transformation $T2$ exists between the two spaces. We assume that the camera's intrinsic parameters are known. Thus, the transformation from $\mathbf{q}$ to $\mathbf{Q}$ in the metric space can be estimated (as shown in the Figure 7). We call $(c_u \quad c_v)$ the optical center on the sensor array, f_c the camera focal length, $(d_u \quad d_v)$ the pixel pitch in the u (resp. v) direction. Neglecting lens distortion, the transformation between $\mathbf{q}$ and $\mathbf{Q}$ is given by:

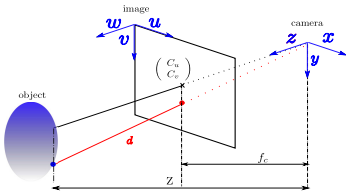

Fig. 7. 2.5D point $\mathbf{q}$ versus 3D point $\mathbf{Q}$

$$T2: \quad \Omega \quad \rightarrow \psi$$
$$\begin{pmatrix} u \\ v \\ d \end{pmatrix} \rightarrow \begin{pmatrix} X \\ Y \\ Z \end{pmatrix} \text{ with } \begin{cases} X = Z\frac{(u-c_u)d_u}{f_c} \\ Y = Z\frac{(v-c_v)d_v}{f_c} \\ Z = d\frac{f_c}{\sqrt{f_c^2+((u-c_u)d_u)^2+((v-c_v)d_v)^2}} \end{cases} \tag{9}$$

where ψ is a subset of $\mathbb{R}^3$: $\psi = [X_{min}; X_{max}] \times [Y_{min}; Y_{max}] \times [Z_{min}; Z_{max}]$. A first order approximation of he variance-covariance matrix $\Sigma^{\mathbf{Q}}$ of $T2$ is given by:

$$\Sigma^{\mathbf{Q}} = \mathsf{J}_{T2} \Sigma^{\mathbf{q}} \mathsf{J}_{T2}{}^{\mathsf{T}}, \tag{10}$$

where J_{T2} is the 3×3 Jacobian matrix of the function $T2$.

4.3 Propagating 3D Uncertainty to Distance Measurement

When making measurements between 3D points $\mathbf{Q}_i$, uncertainty arises from the uncertain localisation of the 3D points modelled by their associated variance-covariance matrix $\Sigma^{\mathbf{Q}_i}$. Here, we are concerned with measurement of the distance between two 3D points. Given two points $\mathbf{Q}_1, \mathbf{Q}_2$ and their associated variance-covariance matrices $\Sigma^{\mathbf{Q}_1}$ and $\Sigma^{\mathbf{Q}_2}$, the distance between $\mathbf{Q}_1$ and $\mathbf{Q}_2$ is defined by the function D:

$$\begin{aligned} D: \quad \psi^2 \quad &\rightarrow \mathbb{R} \\ \begin{pmatrix} \mathbf{Q}_1 \\ \mathbf{Q}_2 \end{pmatrix} &\rightarrow \|\overrightarrow{\mathbf{Q}_1\mathbf{Q}_2}\|_2 \,. \end{aligned} \tag{11}$$

Assuming a statistical independence between $\mathbf{Q}_1$ and $\mathbf{Q}_2$, a first order approximation of the variance σ_D^2 is given by:

$$\sigma_D^2 = \mathsf{J}_D \begin{pmatrix} \Sigma^{\mathbf{Q}_1} & 0 \\ 0 & \Sigma^{\mathbf{Q}_2} \end{pmatrix} \mathsf{J}_D{}^{\mathsf{T}}, \tag{12}$$

where J_D is the 1×6 Jacobian matrix of the function D.

5 Applicative Example

We give a simple example of use of our uncertainty modelling on real data. The TOF camera used is a PMD CamCube2 with a resolution of 204×204 pixels [8]. It is assumed to be calibrated (its internal parameters are known). The example consists in measuring the width and the height of a calibration checkerboard. These measurements are obtained from the 4 points clicked on the image $\mathbf{p}_1, \mathbf{p}_2$ and $\mathbf{p}_3, \mathbf{p}_4$ (see Figure 8(b)). For each 2D point $(\mathbf{p}_i)_{i=1}^4$, the $\Sigma^{\mathbf{p}_i}$ is computed: multiple-clicks are performed and the standard deviation in each direction (u, v) is computed. Then, the corresponding 3D point $(\mathbf{Q}_i)_{i=1}^4$ and their covariance-variance matrix $(\Sigma^{\mathbf{q}_i})_{i=1}^4$ and $\left(\Sigma^{\mathbf{Q}_i}\right)_{i=1}^4$ are computed as explained in Section 4. The first point $\mathbf{p}_1$ is considered as an example to present the uncertainty propagation. The covariance matrices $\Sigma^{\mathbf{p}_1}$, $\Sigma^{\mathbf{q}_1}$ and $\Sigma^{\mathbf{Q}_1}$ are:

$$\Sigma^{\mathbf{p}_1} = \begin{pmatrix} 2.5^2 & 0 \\ 0 & 1.7^2 \end{pmatrix} \Sigma^{\mathbf{q}_1} = \begin{pmatrix} 6 & 0 & 24.7 \\ 0 & 2.9 & 1.3 \\ 24.7 & 1.3 & 154.3 \end{pmatrix} \Sigma^{\mathbf{Q}_1} = \begin{pmatrix} 286.3 & -64.4 & 230.2 \\ -64.5 & 202.9 & -7.9 \\ 230.2 & -7.9 & 275 \end{pmatrix}.$$

From these matrices, the uncertainty ellipse of $\mathbf{p}_1$ (Figure 8(c)) and the uncertainty ellipsoids of $\mathbf{q}_1$ (Figure 8(d)) and $\mathbf{Q}_1$ (Figure 8(e)) are drawn. Then,

the checkerboard width $D(\mathbf{Q}_1, \mathbf{Q}_2)$ and height $D(\mathbf{Q}_3, \mathbf{Q}_4)$ values are computed from Equation (11). Their values are respectively equal to $h = 1250$ mm and $w = 906mm$, the ground truth are respectively 1200 mm and 900 mm. The error between measured and ground truth distances is not only due to sensor noise. The TOF camera are subject to depth distortion [9–11]. There are several causes for depth distortion, one of them is the called *systematic error*. In this paper, this latter is corrected [12]. After width and height computation, their variance values are computed from Equation (12) and the uncertainty (which is equal to standard deviation) are deduced. They are respectively equal to σ_h=28.4 mm and σ_w=17.9 mm. Note that ground truth values fall within the confidence intervals $[h - 2\sigma_h; h + 2\sigma_h]$ and $[w - \sigma_w; w + \sigma_w]$ with levels of confidence [3] equal to 95% and 68%.

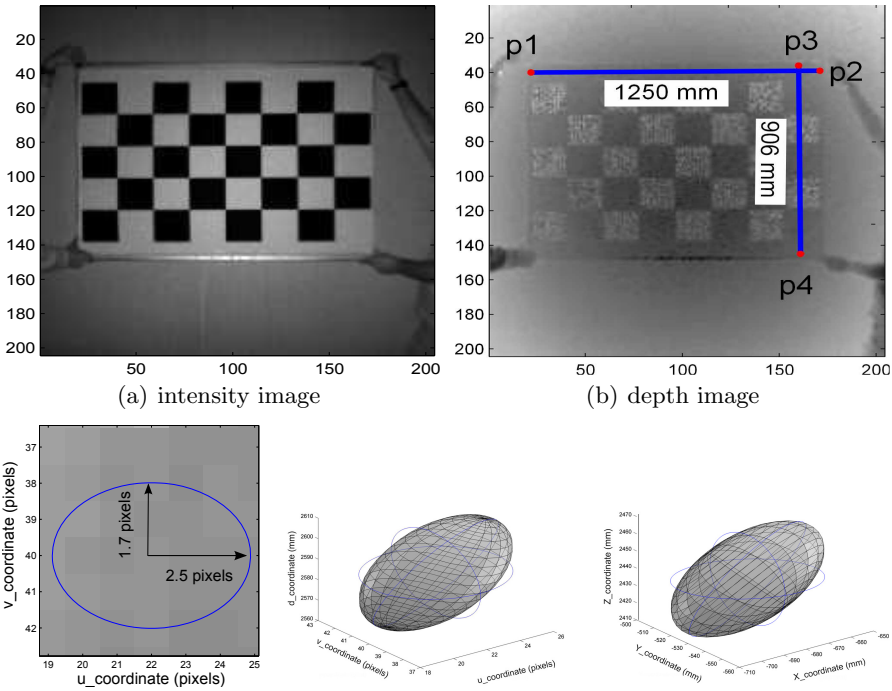

(a) intensity image (b) depth image

(c) $\mathbf{p}_1$ uncertainty ellipse (d) $\mathbf{q}_1$ uncertainty ellipsoid (e) $\mathbf{Q}_1$ uncertainty ellipsoid

Fig. 8. Measuring the checkerboard width and height from depth-pixels: (a) the intensity image and (b) the depth image corrected for radial distortion. Computed width and height are respectively equal to $1250 \pm 28.4mm$ and $906 \pm 17.9mm$. The computed (c) uncertainty ellipse of $\mathbf{p}_1$ and uncertainty ellipsoid of (d) $\mathbf{q}_1$ and (e) $\mathbf{Q}_1$ are presented. The associated uncertainly ellipses are drawn in blue around the ellipsoids.

[3] The level of confidence would indicate the probability that the confidence interval contains the ground truth value. Not that greater levels of confidence give larger confidence intervals, and hence less precise estimates of the parameter.

6 Conclusion

We have characterized the noise distribution of TOF sensors as Gaussian. A 3D Thin-Plate-Spline is used as a noise's standard deviation model. A method that approximates the uncertainty associated to TOF measurements is proposed. A simple example on real data demonstrate an application of the proposed approach. Future work will improve the robustness of TOF algorithms using the uncertainty information. It would also be interesting to test the proposed approach for the Kinect sensor.

References

1. Lange, R.: 3D Time-of-Flight distance measurement with custom solid-state image sensors in CMOS/CCD-technology. PhD thesis, University of Siegen, Germany (2000)
2. Kim, S.Y., Cho, J.H., Koschan, A., Abidi, M.A.: Spatial and temporal enhancement of depth images captured by a time-of-flight depth sensor. In: ICPR (2010)
3. Kim, S.M., Cha, J., Ryu, J., Lee, K.H.: Depth video enhancement for haptic interaction using a smooth surface reconstruction. IEICE - Trans. Inf. Syst. E89-D, 37–44 (2006)
4. Cho, J.H., Chang, I.Y., Kim, S., Lee, K.: Depth image processing technique for representing human actors in 3dtv using single depth camera. In: 3DTV (2007)
5. Zhu, J., Wang, L., Yang, R., Davis, J.: Fusion of time-of-flight depth and stereo for high accuracy depth maps. In: CVPR (2008)
6. Chambers, J.M., Cleveland, W.S., Kliener, B., Tukey, P.A.: Graphical Methods for Data Analysis. Wadsworth (1983)
7. May, S., Droeschel, D., Holz, D., Fuchs, S.: Three-dimensional mapping with time-of-flight cameras. J. Field Robot. 26, 934–964 (2009)
8. PMDTechnologies: Pmd[vision]camcube 3.0 (2009), `http://www.pmdtec.com/products-services/pmdvisionr-cameras/pmdvisionr-camcube-20/`
9. Karel, W., Dorninger, P., Pfeifer, N.: In situ determination of range camera quality parameters by segmentation. In: Opt. 3D Meas. Tech. (2007)
10. Guömundsson, S.A., Aanæs, H., Larsen, R.: Environmental effects on measurement uncertainties of Time-of-Fight cameras. In: ISSCS (2007)
11. Weyer, C.A., Bae, K.H., Lim, K., Lichti, D.D.: Extensive metric performance evaluation of a 3D range camera. In: ISPRS (2008)
12. Belhedi, A., Bourgeois, S., Gay-Bellile, V., Sayd, P., Bartoli, A., Hamrouni, K.: Non-parametric depth calibration of a tof camera. In: ICIP (2012)